RSC Advances

PAPER

View Article Online
View Journal | View Issue

Cite this: *RSC Adv.*, 2024, **14**, 15468

Characterization of cement mortars with regional organic and inorganic additives

Montserrat Soria-Castro, [a] Juan Genescá-Llongueras, [a] Gloria Ivonne Hernández-Bolio [b] and Pedro Castro-Borges *[b]

The present investigation establishes the basis for future studies in the southeast of México for the improvement of building materials by combining regional organic and inorganic nanoparticles in admixtures to formulate cement mortars with durability potential in structures of concrete. The characterization of the organic extract of *Albzia tomentosa* by nuclear magnetic resonance (NMR) revealed the presence of epicatechin (tannin related) and sucrose. Calcium zinc hydroxide dihydrate nanoparticles (CZ NPs) showed the highest surface area of 60.7 m^2 g^{-1}. The electrical resistivity, propagation of ultrasound velocity and water absorption by capillarity properties were individually evaluated for the organic extract, the inorganic nanoparticles and their admixtures in cement mortars, at a curing time of 7, 28 and 96 days with and optimal concentration of 5 mg mL^{-1} of the added additives. The best results were obtained at 96 days showing slightly but clear improvement of the electrical resistivity (23.40 ± 0.022 kΩ cm, 22.40 ± 0.004 kΩ cm and 22.29 ± 0.013 kΩ cm), propagation of ultrasound velocity (1370 ± 10 m s^{-1}, 1345 m s^{-1} ± 6, 1310 ± 9 m s^{-1}) and capillary coefficient (0.0044 kg $m^{-2}s^{-1/2}$, 0.0045 kg $m^{-2}s^{-1/2}$ and 0.0049 kg $m^{-2}s^{-1/2}$) properties of the cement mortars with CZ NPs, extraction *Albizia* solution (EAS) and CZ NPs + EAS respectively when compared to the mortar control (19.91 ± 0.036 kΩ cm, 1266 ± 15 m s^{-1} and 0.0082 kg $m^{-2}s^{-1/2}$).

Received 27th January 2024
Accepted 12th April 2024

DOI: 10.1039/d4ra00690a

rsc.li/rsc-advances

1. Introduction

Cement is the most widely used material in the construction sector worldwide. During the last century, it has shown many advantages, with the main benefits being its low cost and the fact that a lower requirement of industrial development is needed for its production.[1,2] This is especially helpful for less developed countries. OPC (Ordinary Portland Cement) is a mixture of clinker and calcium sulfate in a ratio of approximately 95 : 5%.[3] The mineralogical composition of clinker consists of alite (Ca_3SiO_5), belite (Ca_2SiO_4), tricalcium aluminate ($Ca_3Al_2O_6$) and tetra-calcium aluminoferrite ($Ca_4Al_2O_{10}F_{e2}$).

Among the widely used cementitious materials are concrete, mortars, and pastes, however, each Portland clinker manufactured ton of cement is responsible for high energy consumption and emission of 0.7 and 0.8 ton of CO_2, approximately.[4–6] Also, it is very probable that these values will increase each year as the construction industry aims to renewed and innovative infrastructure to meet the expectations of society. In an effort to reduce these values and lower the impact of global warming, different countries around the world have replaced the OPC with the CPC (Composite Portland Cement) which entails important changes in the source of primary substance during the elaboration of the cement. On the other hand, CPC is eco-friendly, which is also low in clinker content that is partially substituted by some by-products like fly ash or others. Many attempts are currently being made to extend the durability and life cycle of building materials and increase their environmental sustainability with the use of organic and inorganic products.[7–11]

Since pre-Hispanic times, organic additives based on lime mortars were used as coatings for the conservation of architectural elements of the Mayan civilization, since they improve several properties as hardness, porosity, water absorption, and permeability.[12] These organic additives came from the bark of trees as *chakaj* (*Bursera simaruba*), *jabin* (*Piscidia piscipula*), and *chukum* (*Havardia albicans*), among others. Lime mortars were used in various parts of the world to improve their durability[13] until the advent of cement which has several advantages over it. Cement mortar and concrete are used to build structures exposed to aggressive environmental conditions that can lead to deterioration and thereby a reduction of their service life. In recent years, the knowledge demonstrated by the ancient Maya civilization with lime mortars has been used for contemporary purposes: cement mortars with *chukum* resin had been applied, showing that they have waterproof and inhibitory properties

[a]*Unidad de Investigación y Tecnología Aplicadas, UNITA, Facultad Química, UNAM. Parque de Investigación e Innovación Tecnológica, PIIT, 66628 Apodaca, NL, Mexico*
[b]*Departamento de Física Aplicada, Centro de Investigación y de Estudios Avanzados del IPN, Unidad Mérida, Yucatán, Mexico. E-mail: pcastro@cinvestav.mx*

against mold, in addition to having a minimalist natural tone.[14] The Yucatan peninsula possess a distinctive flora particularly rich in Leguminosae species,[15] as the abovementioned, whose treebark is enriched with compounds having a wide array of properties. *Albizia tomentosa* is among these species, a small to medium-sized tree with a rounded crown; its bark is grey/brown and horizontally ribbed.[16] Although no phytochemical studies have been performed, it is expected to have similar polyphenolic compounds which might improve the cement properties.[17]

Conversely, there are constructions with linings and agricultural canals where concrete is prepared near these sectors and mixed with the impurities of flora and fauna in the form of vitamins, proteins, and acids, which become part of the concrete during its formation,[18,19] consequently, Rashid *et al.*[20] evaluated cement mortars at 7, 28, 90 and 180 days (curing time) with three organic materials that can be unintentionally mixed during casting due to contamination in civil construction works. These materials were vinegar, gram pulse, and frog contaminated water, which were evaluated through the mechanical test of compressive strength and the comparison with the reference material. The authors concluded that all these organic products affected its strength, especially at 180 days. Therefore, it is important to select the appropriate organic material in order to have the desired improvement in the properties of cement mortars.

Recently, nanotechnology innovations with scientific and technological applications that benefit from the exchange of information to basic science and society, have exponentially expanded the use of nanoparticles in the construction industry during the last decades.[21,22] Concrete, being a heterogeneous material at all scales and lengths, is an exceptional candidate for the nanomodification of cement-based materials. In addition, nanoparticles are expected to significantly affect the kinetics and hydration reaction of cement and generate pore filling, improving its mechanical properties due to their large surface area and electrostatic attraction.[23] Among the most studied nanoparticles that improve the properties of cement-based materials, nano$CaCO_3$ has proven to accelerate the rate of hydration and improve mechanical properties.[10] Siang-Ng *et al.*[24] reported the influence of SiO_2, TiO_2, and Fe_2O_3 nanoparticles used in the blended cement mortars. The results show that an optimum concentration of nanoparticles incorporated in the mortar, improves the compressive and flexural strengths and by Scanning Electron Microscopy (SEM) has a denser and more compact microstructure compared to control mortar. Also, TiO_2 nanoparticles evaluated in cement mortars of alkali-activated, show an enhancement in the compressive strength, elastic modulus and shows a beneficial effect in self-cleaning capability,[25] due to the photocatalytic properties of TiO_2.[26]

On the other hand, ZnO has been used in cement pastes as admixture but is known that chemical interaction of Zn with the cement clinker grains during hydration retards curing. However, Andrade-Brem *et al.*[27] demonstrated by X-ray diffraction (XRD), Rietveld refined XRD, and SEM that, on day 7 of curing, a crystalline phase of $CaZn_2(OH)_6 \cdot 2H_2O$ was formed, which allowed the hydration of the mixed cement with ZnO and proposed a model to explain these reactions. In this regard, other authors[28] have studied the solubility of $CaZn_2(OH)_6 \cdot 2H_2O$ through the analysis of Zn behavior in cementitious systems. The chemical synthesized compound resulted in a solubility value of $\log K_{s0} = 43.9$, demonstrating that Zn reach the equilibrium with calcium–silicate–hydrate at pH values between 11.7 and 12.78 and an ionic strength of 0.1 M. Nevertheless, the use of $CaZn_2(OH)_6 \cdot 2H_2O$ as an additive for the durability of concrete and cement mortars has not been studied in depth to date.

This work searches the sustainability of concrete through the incorporation of novel additives coming from the regional flora, with plenty of interesting molecules, and locally synthesized nanoparticles to obtain an environmentally friendly construction material. Therefore, the present research aimed to evaluate the durability of cement mortars with organic and inorganic additives. For this purpose, the bark of *Albizia tomentosa* was extracted by maceration in water and then, calcium zinc hydroxide dihydrate nanoparticles with the chemical formula $CaZn_2(OH)_6 \cdot 2H_2O$ (denominated CZ NPs) were obtained by the sol–gel method. These two additives, and the mixture of both, were added to cement mortars to perform the durability tests: electrical resistivity, propagation of ultrasound velocity and water absorption by capillarity. Furthermore, the organic extraction as well as the inorganic nanoparticles, Composite Portland Cement (CPC) and stone powder (agreggates), were characterized by several techniques as SEM, XRD, NMR, TGA (Thermogravimetric analysis) and BET (Brunauer–Emmett–Teller) method in order to know their physicochemical properties. The assessing of these durability parameters, allows to evaluate the feasibility of organic extracts and inorganic nanoparticles as admixtures applied to the construction materials industry.

2. Experimental

2.1 Standards

The Mexican standard of durability NMX-C-530-ONNCCE-2018 [29] provided us with methods, procedures, criteria, *etc.* to be able to design, inspect, diagnose, repair, rehabilitate or reinforce concrete structures or other elements such as mortars and cement pastes with criteria of durability that are subjected to different types of aggressive environments in the country. The interpretation of durability is a product of the correlation between several of its parameters. Some of these parameters that were used in this research were determined by the following standards: NMX-C-077-1997-ONNCCE,[30] NMX-C-514-ONNCCE-2016,[31] NMX-C-275-ONNCCE-2004 [32] and NMX-C-504-ONNCCE-2015.[33]

2.2 Materials

The materials used in this research were CPC, aggregates typical from the region of the Yucatan peninsula, extract from the bark of *Albizia tomentosa*, a tree native to the Yucatan peninsula, and CZ NPs, synthesized by the sol–gel method.

2.3 Sol–gel synthesis of CZ NPs

CZ NPs was synthesized by combining two independent solutions with 100 mL of deionized water (Labconco WaterPro PS, 18 MΩ cm). The first having a concentration of 80 mM NaOH (Aldrich,

Table 1 Data obtained from herbarium entries collected in the Yucatan peninsula

Taxon	Basonym	Common names	Geographic distribution
Albizia tomentosa (Micheli) Standl	*Pithecellobium tomentosum Micheli*	*palo de sangre*, *arrocillo* (*español*); *juub che'*, *sak piich*, *xa'ax* (*maya*)	Campeche, Q. Roo, Yucatán

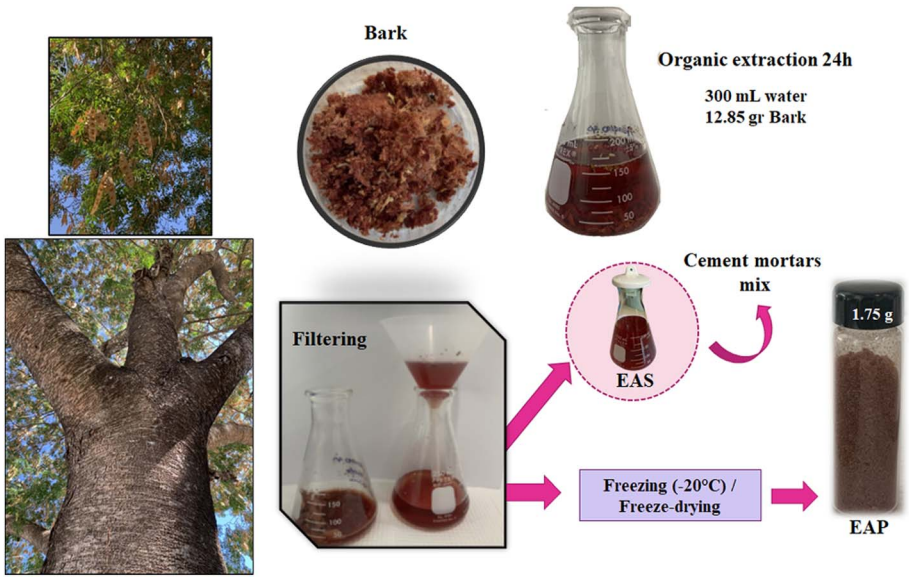

Fig. 1 Methodology for the organic extraction from *Albizia tomentosa* bark.

98%) and 10 mM ZnO and previously synthesized according to the method reported in Gómez-Ortíz *et al.*,[34] while the second being a 9 mM solution of $CaCl_2 \cdot 2H_2O$ (Reasol, 78%). Both solutions were heated and stirred at 90 °C, then mixed and stirred for 5 h at 90 °C. Finally, the resulting solution was washed two times with water (Labconco WaterPro PS; 18 MΩ cm) to remove NaCl; the pH value of the colloidal suspension was 13.

2.4 Organic extraction of the *Albizia tomentosa* bark

The *A. tomentosa* tree is native to the Yucatan peninsula. It belongs to the Fabaceae family as the *chukum* tree. Table 1 shows the taxonomic information available from the flora digital site, the online database of the Centro de Investigación Científica de Yucatán herbarium (CICY, 2023).[35]

The methodology for the extraction consists in obtaining pieces from the bark of the *Albizia tomentosa* tree. The fragments were immediately weighed and placed in deionized water for 24 h to extract the high-polarity compounds. Then, a small volume of the resulting supernatant (red color) was filtered and freeze-dried to obtain the yield of extraction from *Albizia* powder (EAP) per milligram of bark material (5 mg mL^{-1}), and subsequently its physicochemical characterization. The remaining organic extraction solution (denominated EAS) was used for the preparation of cement mortar mixes (Fig. 1).

2.5 Characterization of the additives

2.5.1 NMR profiling of the EAP. The NMR experiments were conducted at 25 °C in a 600 MHz Varian-Agilent AR Premium Compact spectrometer (14.1 T). The EAP was resuspended in 600 μL deuterated water containing 0.05% tsp as a chemical shift reference and transferred to a 5 mm NMR tube. The proton (^1H) and carbon (^{13}C) NMR were recorded for obtaining better results by using the *s2pul* sequence with 128 and 50 000 transients, respectively. Additional 2D-NMR experiments as gHSQC were carried out to support the identification of the detected metabolites.

2.5.2 XRD mineralogical analysis. Powder X-ray diffraction analyses (XRD Siemens D-5000) were performed with a Bragg–Brentano geometry and Cu-Kα radiation ($\lambda = 1.5418$ Å) using the following scan: step size = 0.02°, $t = 3$ s, $10° \leq 2\theta \leq 70°$, and the powder pattern was determined by comparison with the XRD database of the Joint Committee on Powder Diffraction Standards (JCPDS). This technique was used to characterize CZ NPs, aggregates and CPC.

2.5.3 Morphological and elemental composition analysis by SEM. The morphology, particle size, and chemical analysis were corroborated by Field Emission-Scanning Electron Microscopy (FE-SEM, JEOL JSM-7600F) in a microscope equipped with an energy dispersive spectrometer (EDS) at 25 kV. This technique was used to characterize CZ NPs, aggregates and CPC.

CZ NPs were additionally characterized by Transmission Electron Microscopy-Selected Area Electron Diffraction (TEM-SAED, JEOL JEM 2100) operated at 200 kV, with a 0.19 nm resolution.

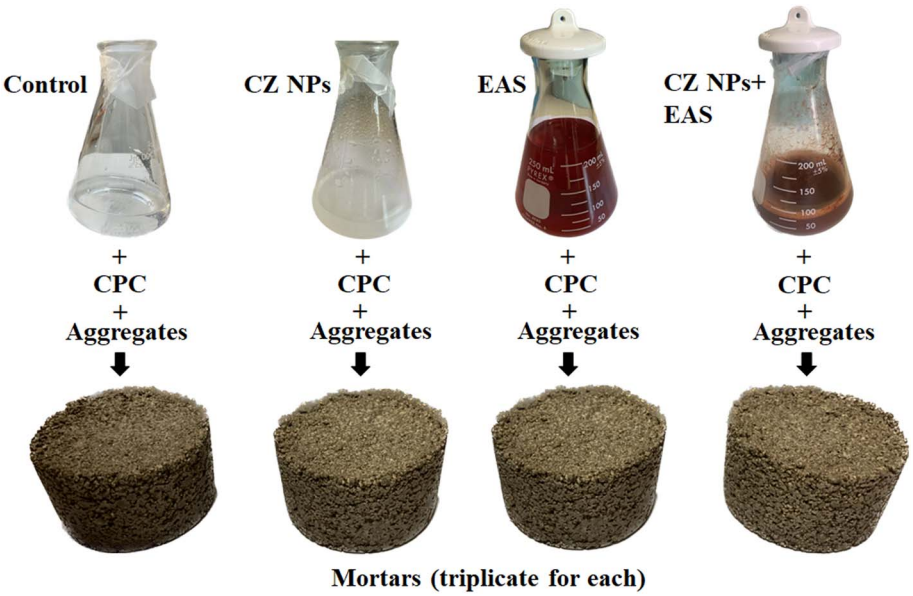

Fig. 2 Diagram of the preparation of mortar mixes for 7, 28, and 96 days of curing.

2.5.4 Textural characterization. The surface characterization of the CZ NPs, EAP, aggregates and CPC was carried out on a BELSORP-Max (Bel Japan, Inc.) instrument. Before each measurement, the sample was degassed under vacuum (7.65 × 10-5 Pa) at 200 °C for 24 h. Subsequently, the measurements were made with N_2 (−196 °C) since it allows analysis of specific surface, volume, and pore size distribution. The specific surface was obtained based on the BET method.[36] In addition, the micropore volume (V_{micro}) together with the mesopore volume (V_{meso}), were evaluated using the t-plot method and the Barrett–Joyner–Halenda (BJH) method, respectively.[37] The mean pore diameter (D_p), was obtained from the following eqn (1):

$$D_p = \frac{4V_T}{S} \quad (1)$$

where V_T is the total volume of pores (summation of V_{micro} + V_{meso}), and S is the BET surface area.[38]

2.5.5 Characterization of TGA. TGA was conducted on a TA-Instruments (Discovery, New Castle, USA) equipment at a heating rate of 10 °C min^{-1} in the temperature range of 25–600 °C for the EAP and 25–800 °C for the aggregates and CPC under air atmosphere with a flow of 25 mL min^{-1}. The percentage of weight loss of the materials was determined using Software TRIOS (v 5.1.0) from TA Instruments.

2.6 Mix proportions of the cement-based mortar preparation

A total of 36 mortar mixes in 6.5 cm × 4 cm sized cylinders were formulated using an aggregates : CPC ratio of (3 : 1). The amount of aggregates was calculated according to NMX-C-077-1997-ONNCCE.[30] The water/cement ratio was 0.5 (w/c). The CZ NPs (5 mg mL^{-1}) and EAS (5 mg mL^{-1}) were incorporated into the solution during the mixing and placed in a silicone mold. Then, after 24 h in the mold, the mortars were removed and placed in a 3% lime solution and left to cure for 7, 28, and 96 days.

The cement-based mortars mixes were prepared as follows: 9 control cement mortars and 9 cement mortars with the CZ NPs in water solution, 9 cement mortars with the EAS, and 9 cement mortars with the mixture of the CZ NPs + EAS (Fig. 2).

2.7 Tests performed on the cement-based mortar mixes

36 mixed proportions of the cement-based mortar were evaluated by the non-destructive techniques that have been established to determine concrete durability, these are electrical resistivity, propagation ultrasound velocity, and water absorption by capillarity. All of these parameters were measured at a cure time of 7, 28, and 96 days to evaluate the improvement in the electrical, physical, and hydric properties of the mortars as a result of the organic and inorganic additives in the mixture.

The electrical resistivity of the mortars by the direct method was measured according to the standard NMX-C-514-ONNCCE-2016.[31] To calculate the resistance to the passage of electric charges Ohm's law was used with the following eqn (2):

$$R_e = \frac{E}{I} \quad (2)$$

where R_e is the electrical resistance (kΩ) which is measured by applying a voltage E and measuring the passage of current I. Electrical resistivity (kΩ cm) was obtained through eqn (3):

$$\rho = R_e k;\ k = \frac{A}{L} \quad (3)$$

where ρ is the electrical resistivity, A is the mortar area (cm^2) and L is the length of the specimen (cm).

Propagation of ultrasound velocity (V_p) was measured to evaluate the improvement in the physical properties of mortars (at higher speed, higher material density, and lower porosity). In this study, V_p was measured as specified in NMX-C-275-ONNCCE-2004,[32] and wave propagation time was measured using a CNS Electronics PUNDIT pulser instrument. Three

measurements were performed in each mortar, through direct transmission/reception mode, across opposite parallel sides of the samples in the three spatial directions (X, Y, Z axis).

Water absorption by capillarity was determined to analyze the hydric behavior through the mortar. This technique shows the amount of absorbed water, expressed by the mass increase of the mortar per unit area for the square root of time (kg m^{-2} $s^{-1/2}$), and the time interval of the amount of absorbed water by the sample was automatically monitored (every 1, 5, 10, 20, 30 min and 1, 2, 3, 4, 5, 6, 24, 48, 72, 96, 120, 144, 168 h) when its lower surface is in contact with the water reservoir, following the procedures described in the standar NMX-C-504-ONNCCE-2015.[33]

3. Results and discussion

3.1 Characterization of the CZ NPs

Powder X-ray diffraction analysis was performed for phase identification. CZ NPs ($Ca(Zn(OH)_3)_2 \cdot 2H_2O$) was identified as the main phase with a relative amount of 92%, also calcite ($CaCO_3$), was detected at around 6% of abundance, and traces of portlandite ($Ca(OH)_2$) were also observed (Fig. 3). These phase proportions are similar to those reported by Soria-Castro *et al.*[39] The presence of calcium carbonate could improve the compatibility of the CZ NPs protective layer when applied to limestone; it can also be present in the aggregates. These nanoparticles have already been tested to determine their diffuse reflectance spectroscopy of 3.1 eV and a particle size of 148.2 nm ± 7.23 and for Z potential a value of −43 mV ± 1.25 and photocatalytic properties with an efficiency of ∼92%.[40,41]

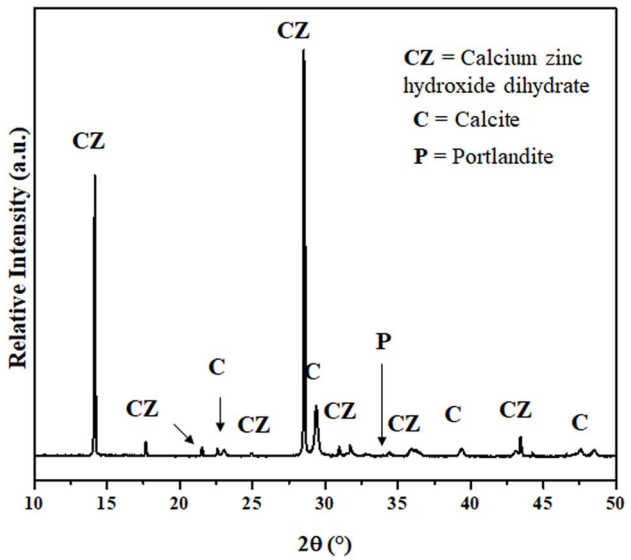

Fig. 3 X-Ray diffractogram for CZ NPs synthesized by sol–gel method.

The morphologies obtained by SEM images of the nanoparticles showed agglomerates (Fig. 4a), while by TEM, the formation of polyhedral structures was observed (Fig. 4b). The measured sizes in both techniques were in the range of 40–100 nm. The electron diffraction inset on TEM analysis shows the identified lattice distance of CZ NPs, as 2.89, 2.81, 2.45 Å, corresponding to the (*hkl*) reflections (−211), (002), (211) (Fig. 4b inset), respectively; which belongs to the monoclinic structure of CZ NPs.

3.2 Characterization of the organic extract EAP

Fig. 5 shows the ^{1}H-NMR spectrum of EAP, where characteristic signals of the flavonoid epicatechin were detected in the aromatic region (6.00–7.50 ppm, circle). Also, broad resonances are observed, suggesting the presence of tannins, which are known to enhance the properties of the mortar.[12,14] Furthermore, signals in the region from 3.00–5.00 ppm were assigned to the sucrose, a disaccharide molecule composed of glucose and fructose. ^{1}H–^{13}C correlations through gHSQC experiment confirmed the molecular structures suggested by ^{1}H-NMR (Tables 2 and 3). The presence of these molecules can substantially improve the properties of construction materials.

Other authors have studied the strengthening and improvement of construction materials through the interaction between natural products and cement hydrates. For instance, Zhang *et al.*[42] added 0.025% tannic acid, a plant-borne polyphenol, to heat-cured cement which resulted in the enhancement of compressive and flexural strengths in cement pastes, by improving the hydration degree of cement and decreasing of porosity as studied by XRD, TGA and SEM. Another recent study uses the tannic acid to treat recycled concrete fines to partially replace Portland cement. Among the benefits of the treatment are the reduction of porosity and cracking of the mortar cement,

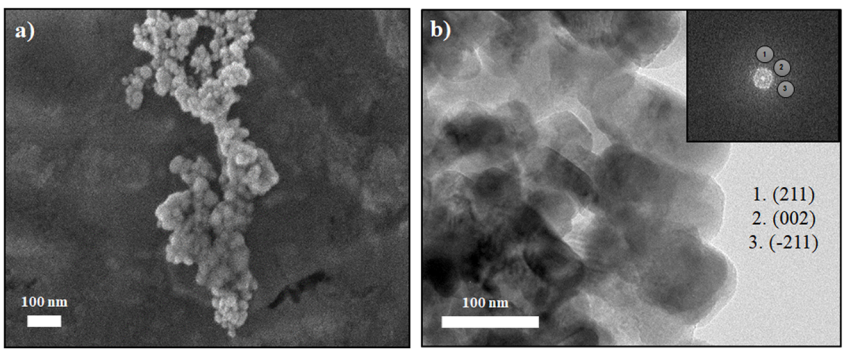

Fig. 4 CZ NPs synthesized by the sol–gel method. (a) SEM images and (b) TEM micrographs (as inset).

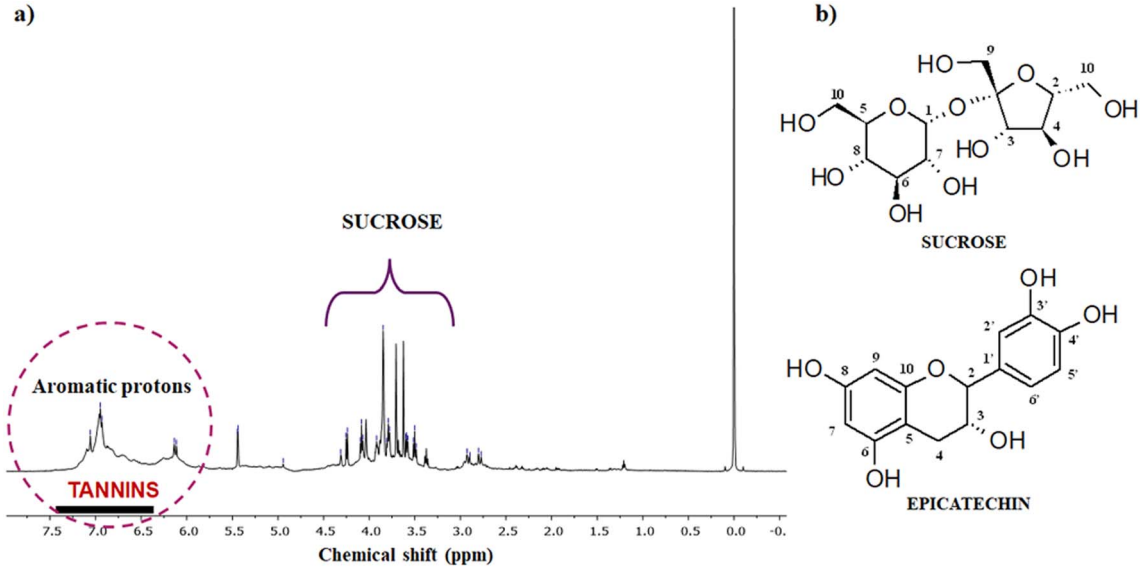

Fig. 5 Characterization of the EAP by ^{1}H-NMR. (a) ^{1}H-NMR spectrum (D_2O, 600 MHz) (b) molecular structures from the main detected metabolites.

Table 2 Signals from sucrose identified from the EAP using ^{1}H, ^{13}C-NMR, and ^{1}H–^{13}C HSQC experiments (D_2O, 600 MHz)

		Chemical shift δ, ppm		
Metabolite	Carbon	^{1}H (multiplicity, coupling constant J)	HSQC (^{1}H–^{13}C)	^{13}C
Sucrose[a]	1	5.44 (d, J = 3.4 Hz)	95.1	
	2	3.93 m	84.2	
	3	4.25 (d, J = 8.7 Hz)	79.3	
	4	4.09 (t, J = 8.6 Hz)	76.9	
	5	3.79 m	75.3	
	6	3.88 m	75.4	
	7	3.59 (dd, J = 9.9, 3.8 Hz)	73.9	
	8	3.51 (t, J = 9.4 Hz)	72.1	
	9	3.71 m	64.2	
	10	3.62 m	63.0	
	11	3.85 m	65.2	

[a] ^{1}H and ^{13}C-NMR assignment based on *Human metabolome database* 2023.[44]

enhancing, at the same time, the packing density of the hydration products, *etc.*[43]

The TGA profile for the organic extract involves two main thermal events (Fig. 6); the first occurs between 30 and 150 °C, mainly related to dehydration processes, with a weight loss of 14%. The second and final step is essentially related to decomposition processes. The first decomposition of 9% weight loss occurs in the range of 153–270 °C; in this stage, it is assumed that sucrose is lost, since their similarities in thermal properties when compared to a pure glucose standard (Sigma-Aldrich) which showed to decompose at 220 °C.

The last decomposition corresponds to a weight loss of 76% and it is attributed to the tannins, beginning at 273 °C up to 525 °C, as Méndez-Figueroa *et al.*[46] reported that the loss between 300 and 600 °C, is attributed to the oxidation of carbon residues. The maximum decomposition temperature values are 52 °C water loss (vertical pink line), 250 °C for sucrose (vertical green line), and 419 °C for tannins (vertical red line).

3.3 Characterization of the aggregates

The results of the granulometry analysis are shown in Fig. 7, which presents the graph in relation to the percentage of the weight of aggregates passing through the corresponding sieve number. The aggregates (blue curve) meets the NMX-C-077-

Table 3 Signals from epicatechin identified from the EAP using ^{1}H, ^{13}C-NMR, and ^{1}H–^{13}C HSQC experiments (D_2O, 600 MHz)

		Chemical shift δ, ppm		
Metabolite	Carbon	^{1}H (multiplicity, coupling constant J)	HSQC (^{1}H–^{13}C)	^{13}C
Epicatechin[a]	2	4.94 s	81.0	
	3	4.31 s	68.5	
	4	2.91 (dd, J = 16.8, 4.0 Hz)	30.3	
		2.79 (dd, J = 16.8, 3.3 Hz)		
	5			157.6
	6	6.14 (d, J = 2.1 Hz)	98.8	
	7			158.2
	8	6.11 (d, J = 2.1 Hz)	98.1	
	9			157.9
	10			102.6
	1′			133.9
	2′	7.06 s	117.3	
	3′			146.7
	4′			148.5
	5′	6.95 s	118.9	
	6′	6.95 s	121.8	

[a] ^{1}H and ^{13}C-NMR assignment based on Natsume *et al.*[45]

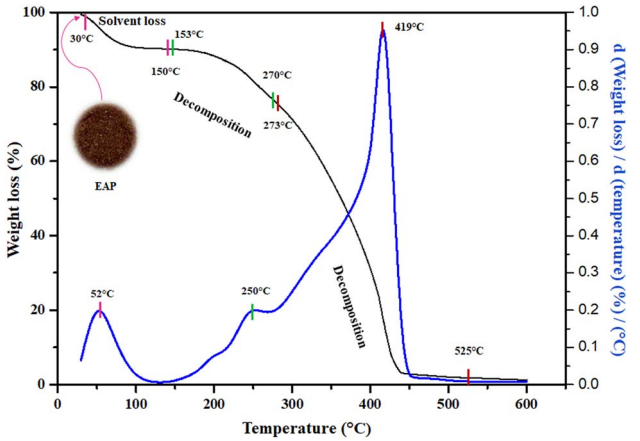

Fig. 6 TGA curve for EAP (black) and its first derivative curve (blue).

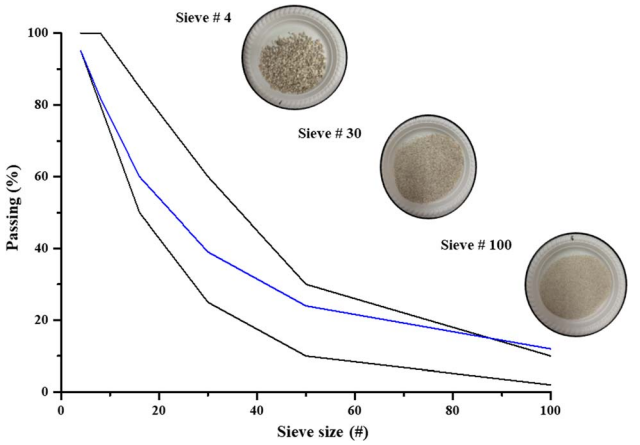

Fig. 7 Granulometry characterization of the aggregates and examples of the sieve size.

1997-ONNCCE[30] (black curve) standard limits for fine aggregates (fineness modulus = 2.8), thus confirming that it can be considered optimal for construction. Besides providing information about the quality of the material, the characterization of the aggregates allowed to know the amount in weight (according to the sieve size) that should be placed to prepare each mortar (final mixture of stone powder according to the sieve).

The X-ray diffractogram of the aggregates (Fig. 8a) shows, as the only mineralogical phase, calcite peaks corresponding to calcium carbonate, which is the typical limestone of the Yucatan peninsula. Interestingly enough, this building material has been used since Mayan, pre-Hispanic, colonial, and modern periods.[47]

The TGA curve of the aggregates showed two mass losses (Fig. 8b). The first one (2%) is attributed to the organic material: the calcite mineral used comes from the stone powder found in the Yucatan region, therefore, it could have low concentrations of organic material (plants, leaves, insects, *etc.*). The second important loss (41%) occurs between 500 and 760 °C with a maximum decomposition temperature value of 720 °C, which corresponds to the $CaCO_3$ releasing of carbon dioxide (CO_2) during heating (decarboxylation).[48] Finally, the remaining compound was CaO.

3.4 Characterization of the CPC

Fig. 9a shows the XRD diffractogram representing the mineralogical composition of the cement: the main peak corresponds to calcite, followed by tricalcium silicate ($3CaO \cdot SiO_2$), also known as alite (C3S), which form hydration products. Also, less abundant phases of anhydrite ($CaSO_4$), an inductor of hydatration, and hatruite (Ca_3SiO_5), form of C3S, were found, as well as traces of dolomite ($CaMg(CO_3)_2$) and goethite (FeO(OH). Their presence could be due to a natural reaction.[49] Regarding its thermal properties (Fig. 9b), the CPC undergoes a continuous sequence of decomposition reactions: the first weight loss (2%), located between 80–200 °C, is corresponding to water. Also, at this temperature the dehydroxylation of goethite takes place, yielding hematite as the dehydrated product.

The second major weight loss (15%), appears at 350–720 °C and corresponds to the decarboxylation of $CaCO_3$ and $CaMg(CO_3)_2$. The residue compounds were C3S, $CaSO_4$, Ca_3SiO_5, CaO, MgO, and Fe_2O_3. The analysis of the first derivative curve gave a maximum decomposition temperature of 80 °

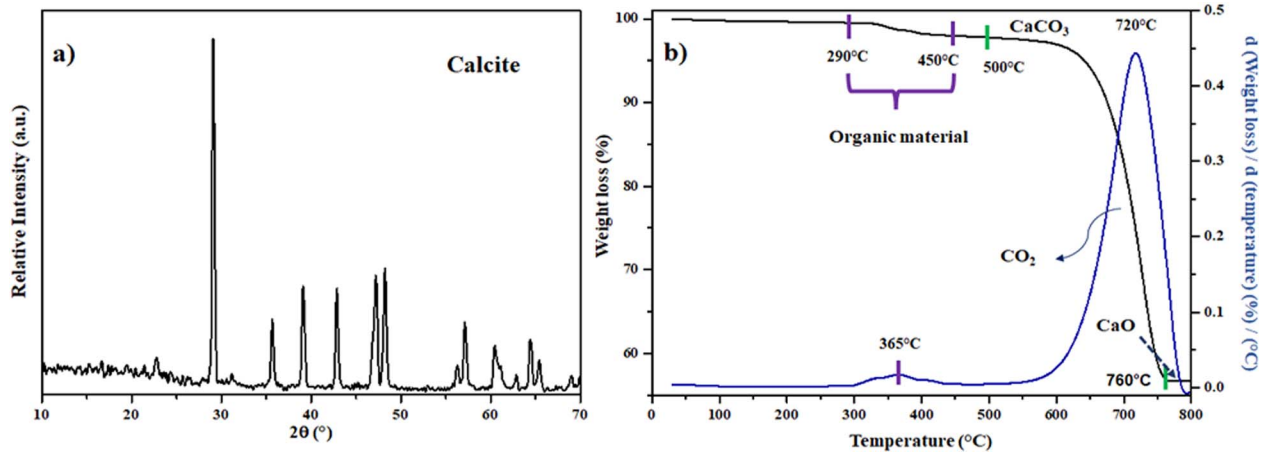

Fig. 8 Characterization of the aggregates: (a) X-ray diffractogram and (b) TGA (black) and its first derivative curve (blue).

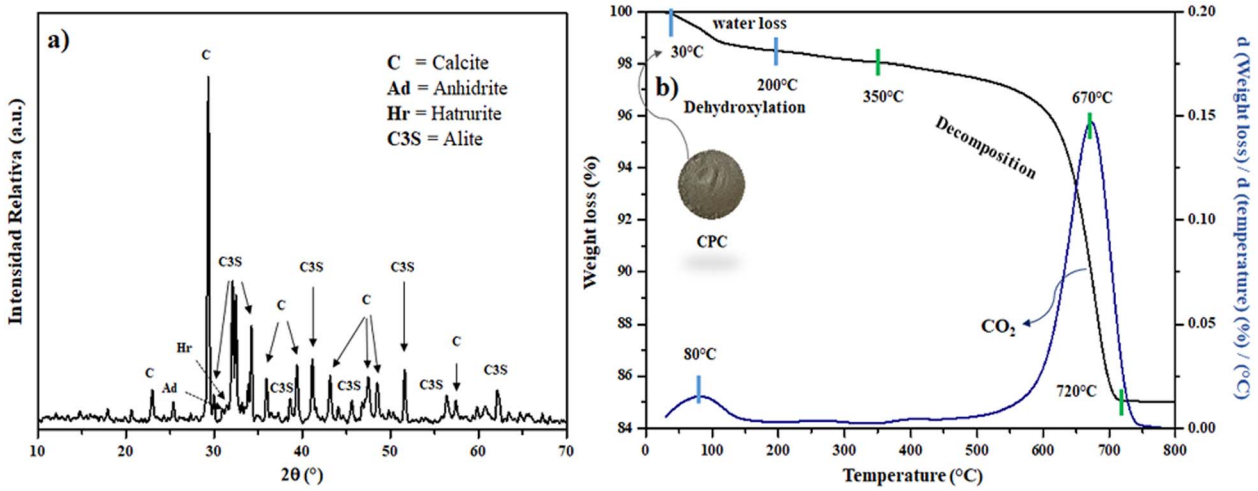

Fig. 9 Characterization of the CPC (a) X-ray diffractogram and (b) TGA (black) and its first derivative curve (blue).

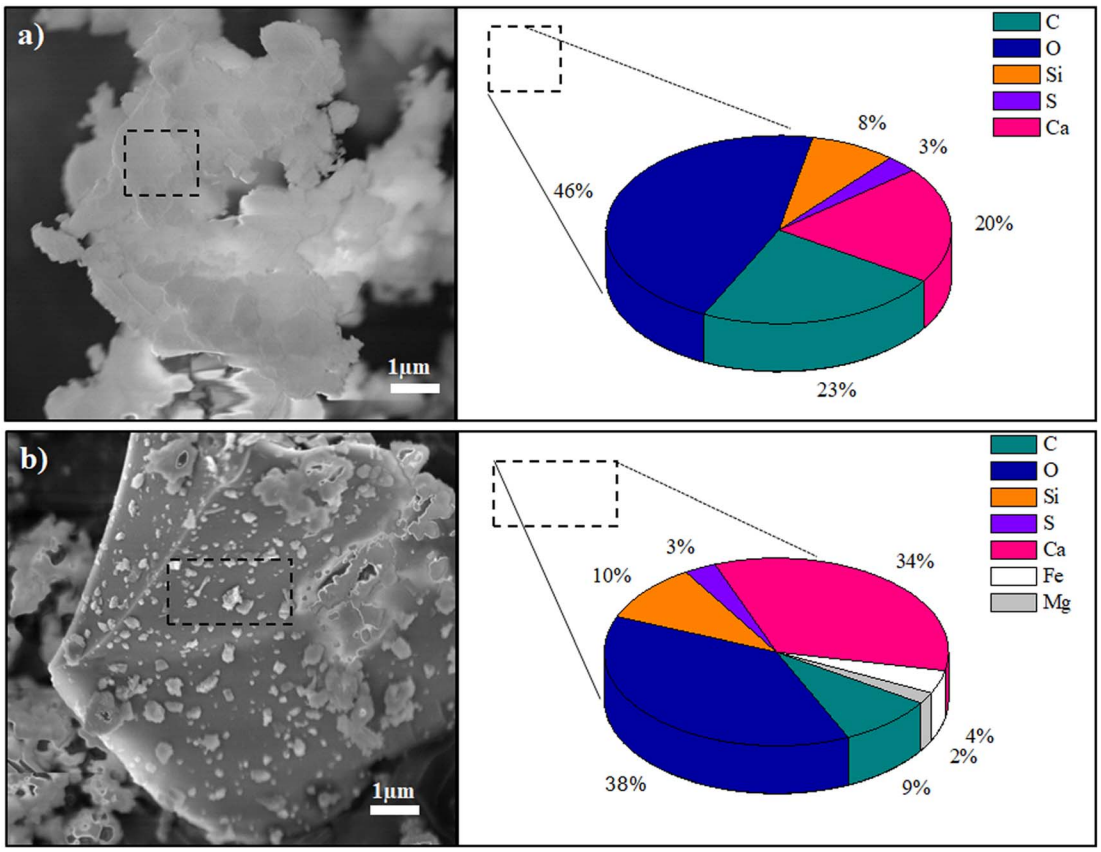

Fig. 10 Characterization of the CPC by SEM image and EDS pattern in two different zones (a) and (b).

C (blue line) water loss, and 670 °C for decarboxylation (vertical green line).

Fig. 10 shows the SEM images of the CPC and its elemental composition in two different zones, (a) and (b), with different characteristics. In zone (a) an amorphous shape is observed although morphologically difficult to define, and zone (b) shows a large particle size of approximately 7 μm with embedded smaller cubic and agglomerated particles between 0.1 and 0.5 μm observed.

Elemental analysis showed the chemical composition of zone (a) to be 23% C, 46% O, 8% Si, 3% S and 20% Ca and for zone (b), the elements 9% C, 38% O, 10% Si, 3% S, 34% Ca and 4% Mg were found, in addition, the trace element Mg (2%) was detected. The elements present in CPC confirmed the compounds detected by XRD.

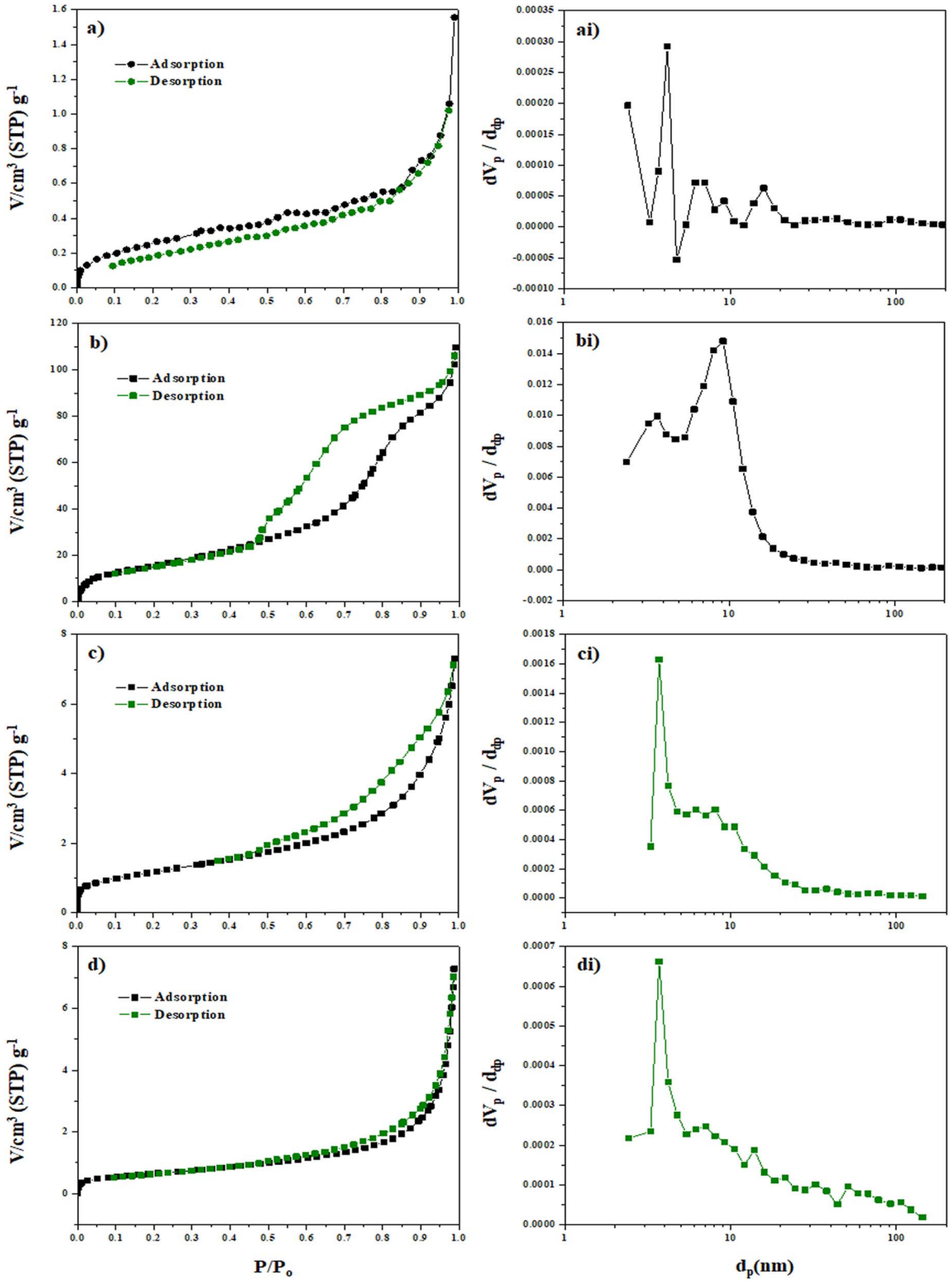

Fig. 11 Nitrogen adsorption–desorption isotherm and pore size distribution of CZ NPs (a and ai, respectively), EAP (b and bi, respectively), Aggregates (c and ci, respectively), and CPC (d and di, respectively).

Table 4 Textural properties of CZ NPs, EAP, aggregates and CPC

	S_{BET} ($m^2\ g^{-1}$)	V_{meso} ($cm^3\ g^{-1}$)	V_{micro} ($cm^3\ g^{-1}$)	V_T ($cm^3\ g^{-1}$)	D_p (nm)	V_{meso}/VT (%)
CZ NPs	60.7	1.7×10^{-1}	9.46×10^{-2}	1.8×10^{-1}	12	94
EAP	0.98	2.27×10^{-3}	1.27×10^{-4}	2.39×10^{-3}	10	95
Aggregates	4.25	1.08×10^{-2}	—	1.08×10^{-2}	11	100
CPC	2.37	1.14×10^{-2}	—	1.14×10^{-2}	19	100

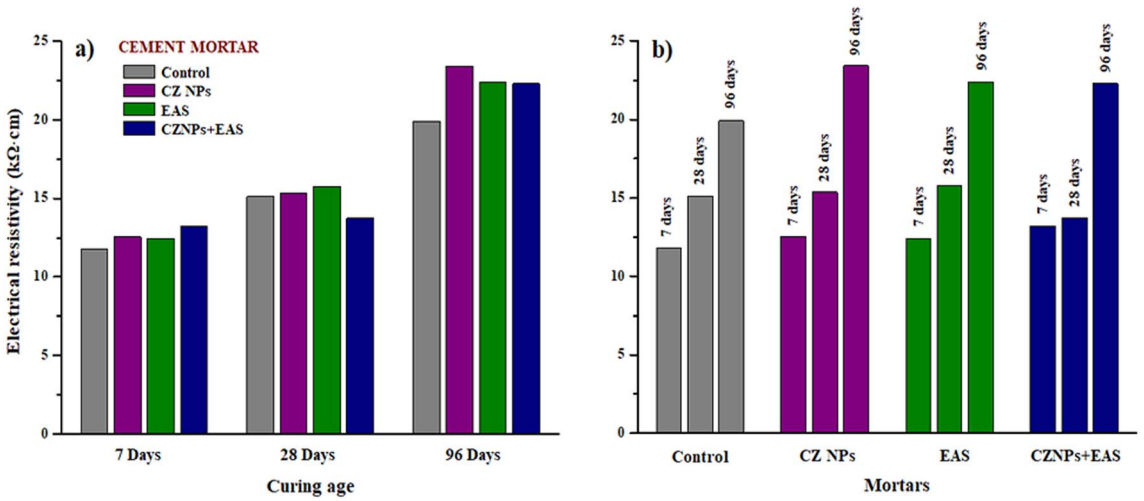

Fig. 12 Comparison of electrical resistivity (kΩ cm) values of cement-based mortar mixes and cured for 7, 28, and 96 days.

3.5 Textural characterization of the CZ NPs, EAP, aggregates, and CPC

The specific surface area was calculated by the BET method and the results are presented in Fig. 11. The N_2 adsorption–desorption isotherm for all the samples exhibits a typical adsorption curve of IV type according to the qualitative classification BDDT (S. Brunauer, LS Deming, WE Deming y E. Teller) indicating mainly the contribution of mesoporous structures. The type of hysteresis cycle is H3, which corresponds to aggregates particles where the plateau in the curve is the product of capillary condensation.[50] Furthermore, the average pore size distribution was determined by the BJH method. Fig. 11(ai and bi) shows the adsorption curve (black) which has a cylinder-shaped pore while Fig. 11(ci and di) shows the desorption curve (green) with a distribution of bottleneck pore.

Table 4 shows the textural characteristics of all samples, the highest surface area was 60.7 $cm^2\ g^{-1}$ for CZ NPs with a V_{meso} of 1.7×10^{-1} $cm^3\ g^{-1}$. The EAP, aggregates, and CPC showed surface area values of (0.98, 4.25, and 2.37 $m^2\ g^{-1}$), and mesopore volume (2.27×10^{-3}, 1.08×10^{-2} and 1.14×10^{-2} $cm^3\ g^{-1}$, respectively).

The pores for all the samples are located in the range of mesoporous (2–50 nm).[50] The mean pore diameter obtained for each material was 12 nm with 94% mesoporous for CZ NPs and 10 nm with 95% mesoporous for EAP. However, the aggregates and the CPC are both 100% mesoporous with a size of 11 and 19 nm, respectively (Table 4).

3.6 Characterization of the electrical, physical, and hydric properties of cement-based mortar mixes

The electrical resistivity for the cement mortar mixes of CZ NPs, EAS, and CZ NPs + EAS was, 12.55 ± 0.013, 12.44 ± 0.015, and 13.21 ± 0.026 kΩ cm respectively, all mixes increased regarding the control (11.77 ± 0.022 Ω) at a curing time of 7 days, this same increasing trend occurs at 28 and 96 days of curing for the values of the control (15.13 ± 0.015, 19.91 ± 0.036 kΩ cm), CZ NPs (15.35 ± 0.027, 23.40 ± 0.022 kΩ cm), EAS (15.75 ± 0.002, 22.40 ± 0.004 kΩ cm) and CZ NPs + EAS (13.73 ± 0.017, 22.29 ± 0.013 kΩ cm) (Fig. 12a). He *et al.*[51] attribute this effect to the fact that, in the early stages of curing, the pores within the mix can be used as an internal conductive pathway, which results in a higher electrical conductivity and in contrast a decreasing resistance. In this sense, with increasing curing age it can be observed that the values increase (Fig. 12b).

As well known, the resistivity of the control cement mortar is related to the continuous hydration reaction of the cement, *i.e.* the presence of tricalcium silicate in this CPC confirmed by XRD, react with water to form calcium silicate hydrate and calcium hydroxide as their principal hydration products.[52] Another optimum compound detected in CPC is calcium sulfate (anhydrite), which is reported to induce the hydration of C3S.[6] and for having adhesive and cohesive properties that are capable of binding together mineral fragments in the presence of water, therefore helping to form a more compact and dense cement mortar. The presence of the mineral hatruite, which is

Table 5 Average values V_p of the cement mortar mixes

Curing	m/s	Control	CZ NPs	EAS	CZ NPs + EAS
7 days	V_p	973 ± 32	1008 ± 16	1006 ± 12	1012 ± 19
28 days	V_p	1025 ± 10	1089 ± 9	1056 ± 5	1013 ± 6
96 days	V_p	1266 ± 15	1370 ± 10	1345 ± 6	1310 ± 9

a form of tricalcium silicate, could be assumed to have the same effect. Also, XRD shows peaks of carbonates such as $CaCO_3$ (major peak) and $CaMg(CO_3)_2$ (trace) which upon hydration start to chemically react into calcium hydroxide and magnesium hydroxide according to the curing time. This explains why the resistivity values of the control mortars is lower than the mixtures with CZ NPs, EAS and CZ NPs + EAS.

Likewise, for CZ NPs cement-based mortars, the results for electrical resistivity according to the curing ages of 7, 28, and 96 days were 12.55 ± 0.013, 15.35 ± 0.027, and 23.40 ± 0.022 kΩ cm, respectively, the latter being the highest resistivity for all mortar mixes. The little improvement in their electrical characteristics can be attributed to the fact that CZ NPs is a small nanomaterial (size from 40 nm) formed by a part of calcium hydroxide which promotes the acceleration of internal hydration and acts as a filler. As previously mentioned, these products could contribute to the effect of filling internal pores in the cement mortar.[27,52] In addition, the increase in the resistivity could be due to the surface area value of CZ NPs (60.7 $m^2 g^{-1}$), which is higher when compared to the values of aggregates and CPC (4.25 and 2.37 $m^2 g^{-1}$, respectively) with mesoporous pores (Table 5). Therefore, CZ NPs would be forming crystalline nucleus in the micropores to densify the cement mortar matrix.

For the EAS cement mortars the electrical resistivity value at 7 days was 12.44 ± 0.015, at 28 days 15.75 ± 0.002, and at 96 days was 22.40 ± 0.004 kΩ cm, which is lower than that of CZ NPs. The tannins and sucrose present in the EAS at a concentration of 5 mg mL^{-1} possibly decreased the formation of cracks, this can be observed by the increase in its resistivity and the standard deviation that shows a higher stability in the data. In a similar way, García-Solís *et al.*[12] have conducted studies with lime mortars using them as organic additives with *chukum* extract. This tree from the Fabaceae family as well as *A. tomentosa*, produces a red color solution when extracted with water and this color is attributed to the high content of tannins, which might be responsible for improving the properties of the lime mortars in terms of their porosity (38.9%), density (1.63 g cm^{-3}), and water absorption (0.02191 g $cm^{-2}s^{-1/2}$) when compared to the control (38.1%, 1.54 g cm^{-3} and 0.02681 g $cm^{-2}s^{-1/2}$).[12] Regarding the mechanism of action, it is possible that the polymerization of tannins, and other polyphenols, lead to an increase in molecular size, thus filling micro cracks produced during the hydration of cement and enhancing properties as compressive strength and modulus of elasticity of concrete, as seen for admixtures of grape and mulberry extracts.[53] In the other hand, the use of sucrose at an appropriate concentration increased the compressive strength of the mortars at 28 days and it showed to be compacted and denser by

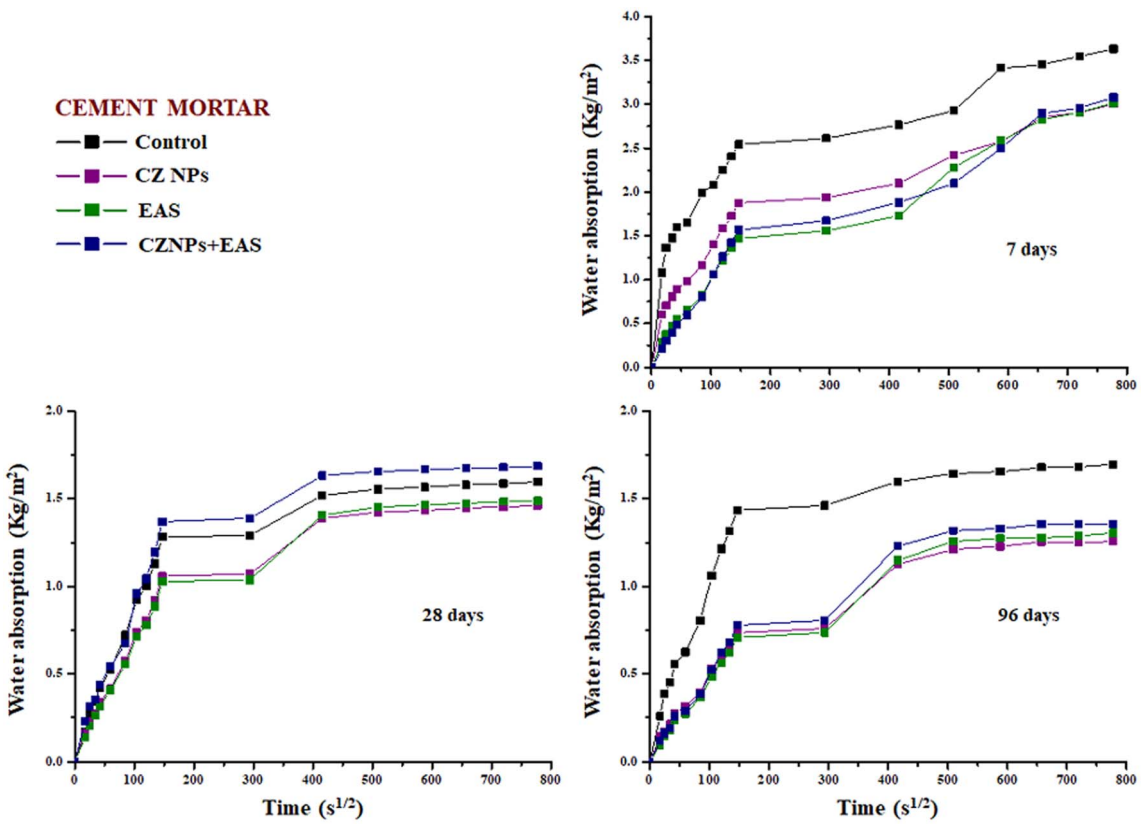

Fig. 13 Capillarity curves obtained during water absorption of cement mortars mixes and cured for 7, 28, and 96 days.

Table 6 Capillary coefficient values of cement mortar mixes

	Control	CZ NPs	EAS	CZ NPs + EAS
Curing	(kg $m^{-2}s^{-1/2}$)	(kg $m^{-2}s^{-1/2}$)	(kg $m^{-2}s^{-1/2}$)	(kg $m^{-2}s^{-1/2}$)
7 days	0.0123	0.0088	0.0085	0.0090
28 days	0.0081	0.0066	0.0065	0.0084
96 days	0.0082	0.0044	0.0045	0.0049

SEM analysis[54] while at low concentrations, delayed the setting time of the pastes by reduction of the C3S hydration and without significant changes in the yield stress evolution.[55] Consequently, the enhancement of the physical durability properties could be due to the presence of the tannins and other polyphenols as epicatechin, which tend to form solid structures, decreasing the porosity in the mortar.

The CZ NPs + EAS mortars could have the same behavior as the cement mortars with CZ NPs and the mortars with EAS, however, the mixture of both organic and inorganic compounds obtained the highest resistivity value at 7 days (13.21 $\pm$ 0.026 kΩ cm), this because it could work as an accelerator of hydration. Subsequently, its increasing growth rate value was lower at 28 days (13.73 $\pm$ 0.017 kΩ cm) and lower regarding the control, however, at 96 days it was higher (22.29 $\pm$ 0.013 kΩ cm) (Fig. 12). The same phenomenon occurred with the ultrasound velocity values (see Table 5).

Table 5 shows that the low values correspond to a curing time of 7 days and the highest values to 96 days. Incorporating CZ NPs, EAS, and CZ NPs + EAS into the cement mortar improved its physical durability properties by filling the internal pores, making the sample more homogeneous and compact gradually, regarding the increase of its ultrasound velocity from 7 to 96 days, according to its anisotropy in the three spatial directions (X, Y, Z axis). These results of the V_p confirmed the results of electrical resistivity, as it improves the physical durability properties of cement mortars when mixed with the tested organic and inorganic admixtures where curing time was also an important factor in increasing its V_p (Table 5).

Fig. 13 shows the water absorption curves, which represent the mass of the cement mortar (kg m^{-2}) as a function of the square root of the time ($s^{1/2}$), with these data its capillarity coefficient was obtained.

From the results of capillarity coefficient, it could be observed that the mixtures with CZ NPs, EAS and CZ NPs + EAS, obtained lower water absorption in the curing times of 7, 28 and 96 days regarding the control cement mortar, respectively (Fig. 13 and Table 6), except for the mortars with CZ NPs + EAS at 28 days of curing (0.0084 kg $m^{-2}s^{-1/2}$). However, after 96 days these values decreased (0.0049 kg $m^{-2}s^{-1/2}$). This could be due to the fact that in a mixture involving inorganic and organic materials, as the organic extract and the inorganic nanoparticles, the adaptation process is slower. The same behavior was obtained for the electrical resistivity and propagation of ultrasound velocity tests.

Since cement mortars with CZ NPs showed the lowest value of the capillarity coefficient (0.0044 kg $m^{-2}s^{-1/2}$), we conclude that the nanometric size of the additive fills the pores of the internal structure of the cement mortar thus helping avoid water transport by capillary action. Also, having a larger surface area improves the interaction of the nanoparticles with the other materials included in the production of the mortar.

The cement mortar with EAS had a value very close to that the samples with CZ NPs (Table 6). The mechanism of action could be influenced by capillary forces (surface tension, adhesion and cohesion),[56] but several studies are needed to confirm this hypothesis.

These results are very important for the civil industry, given that mortars, being a building material that can be exposed to the tropical environment, the absorbed water commonly contains high concentration of soluble salts (Cl^-, SO_4^{2-}) and those ions will certainly have a destructive effect in reinforced concrete.[57]

In addition to its concrete improvement properties, the presence of CZ NPs in the cement mortar mixtures could be exerting a beneficial effect in self-cleaning capability, given that has been reported their remarkable photocatalytic activity (efficiency of ~92%).[40] Furthermore, it has been shown that these NPs have antimicrobial properties when applied to limestone.[34,41] From the side of organic additives, it is also reported that the bioactive compounds from the extracts of another *Albizia* species were used in the biosynthesis of zinc oxide nanoparticles, showing strong antibacterial and antioxidant activities.[58] Also, in a recent investigation, the aromatic hydroxyl rings of *Mimosa* (Fabaceae) tannins have been used to form nanocontainers of ZnO applied to steel as a self-healing coating.[46] These additional features, together with the properties mentioned above, outline the present organic and inorganic additives in this region as ideal materials which can be used as an improved method for the durability of reinforced concrete structures exposed to microbial environments. Moreover, TGA analysis showing the decomposition phases of the compounds, was used to study the temperature limits of these materials to be applied in civil construction.

These experiments established the basis of further work in order to investigate the mechanical properties of the additive-enhanced cement mortars *e.g.* compressive strength tests, which will be carried out together with complementary studies on the durability of concrete structures.

4. Conclusions

From the experimental study using CZ NPs and EAS as additives for the improvement of properties of cement mortars, during the curing time of 7, 28 and 96 days, the following conclusions can be drawn:

The characterization of the materials CZ NPs, EAP, aggregates, and CPC used for the preparation of the cement mortar mixtures was beneficial since knowing their organic and mineralogical composition, size, morphology and surface area, helped to explain the reaction processes and the formation of the hydration products such as calcium hydroxide from the mineral alite.

For the electrical resistivity and propagation of ultrasound velocity tests, it was concluded that the addition of CZ NPs and EAS on cement mortars led to an improvement of their properties, as they play an important role as accelerators of cement hydration, which in the case of nanoparticles it could be due to the $Ca(OH)_2$ incorporation of $CaZn_2(OH)_6 \cdot 2H_2O$ compound (CZ NPs).

The size of the CZ NPs and the larger surface area value compared to the other materials enhanced the interaction regarding the pore filling in the internal structure of the mortar. For the epicatechin and sucrose molecules, as well as tannins, the action mode is yet unknown, however, the significant results obtained in this investigation stimulate the interest in future studies regarding the use and the mechanism of organic additives in mortar mixes.

In general, the results of water absorption are highly correlated to the results of the analytical techniques described above, *e.g.* the higher the resistivity of cement mortar with organic and inorganic additives, the higher its resistivity, the lower its porosity, and the lower its capillary coefficient. However, the cement mortars with the CZ NPs + EAS mixes at 7 days of curing had the best resistivity and ultrasound velocity with low water absorption, but at 28 days, they behaved slightly inferior than the control, but at 96 days they again behaved better than the control.

The water absorption by capillarity, the low electrical resistivity and the high porosity are a very significant problem in building materials. Therefore, these nanoparticles and organic extracts applied in cement mortars could be an ideal method for the durability of concrete structures.

Author contributions

Montserrat Soria-Castro: investigation, methodology, preparation and characterization of materials and writing original draft. Juan Genescá-Llongueras: conceptualization, supervision and funding acquisition. Gloria Ivonne Hernández-Bolio: organic extraction and methodology by NMR. Pedro Castro-Borges: data curation, review & editing, project administration and resources. All authors have read and agreed to the published version of the manuscript.

Conflicts of interest

There are no conflicts to declare.

Acknowledgements

One of the authors, Montserrat Soria Castro, is grateful for the postdoctoral financial support of the Dirección General de Asuntos del Personal Académico [DGAPA] through the project, "Programa de Becas Posdoctorales en la UNAM", and thanks to Faculty of chemistry from UNITA-UNAM, Monterrey N. L. host institution. The authors also acknowledge to Ing. Mercedes Balancan Zapata for her valious help in the understanding and measurement of cement mortar, as well as to M. C Alexia Zozaya Ortiz for her assistance in capillarity tests at CINVESTAV, Mérida. Thanks also to Dra. Patricia Quintana Owen responsible of Laboratorio Nacional de Nano y Biomaterials (*LANNBio*) from CINVESTAV, Mérida for the use of laboratories and their characterization instruments, in particular to Dr Santiago Gonzalez for the BET characterization. Also, we thank L. Díaz Flores for his support with TEM-SAED (Tabasco Science and Applied Technology Reserch Center).

References

1 Cembureau, *Activity Report, Built in Concrete. Made with Cement*, Brussels, 2018.
2 D. D. L. Chung, Functional properties of cement-matrix composites, *J. Mater. Sci.*, 2001, **36**, 1315–1324.
3 A. Nonat, *Chapitre2: L'hydratation des ciments-La durabilité des bétons*, 2008.
4 C. Li, X. Z. Gong, S. P. Cui, Z. H. Wang, Y. Zheng and B. C. Chi, *CO_2 Emissions Due to Cement Manufacture*, Materials Science Forum: Trans Tech Publ., 2011, pp. 181–187.
5 R. M. Andrew, Global CO_2 emissions from cement production, 1928–2017, *Earth Syst. Sci. Data*, 2018, **10**, 2213–2239.
6 K. Cabrera-Luna, E. E. Maldonado-Bandala, D. Nieves-Mendoza, P. Castro-Borges, P. Perez-Cortes and J. I. Escalante García, Supersulfated cements based on pumice with quicklime, anhydrite and hemihydrate: Characterization and environmental impact, *Cem. Concr. Compos.*, 2021, **124**, 104236, **https://www.sciencedirect.com/journal/cement-and-concrete-composites**.
7 W. Schmidt, I. L. Tchetgnia Ngassam, K. A. Olonade, R. Mbugua and H. Kühne, *Plant Based Chemical Admixtures – Potentials and Effects on the Performance of Cementitious Materials*, RILEM Technical Letters, 2018, vol. 3, pp. 124–128.
8 P. R. Kalyana-Chakravarthy, T. Ilango and R. Pugazhenthi, Mechanical properties of concrete with foundry sand andcoconut shell as partial replacement for coarse and fine aggregate, *Mater. Today: Proc.*, 2022, **52**, 537–543.
9 L. Dvorkin, O. Dvorkin, Y. Garnitsky and Y. Ribakov, Adhesive and cohesive properties of glue cement mortars with addition of organic–mineral modifiers, *Mater. Des.*, 2014, **53**, 588–595.
10 T. Sato and F. Diallo, Seeding effect of nano-$CaCO_3$ on the hydration of tricalcium silicate, *J. Transp. Res. Board*, 2010, **2141**, 61–67.
11 E. Ghafari, S. A. Ghahari, Y. Feng, F. Severgnini and N. Lu, Effect of zinc oxide and Al–zinc oxide nanoparticles on the rheological properties of cement paste, *Compos. B Eng.*, 2016, **105**, 160–166.
12 C. A. García-Solís and Y. Jáidar Benavides, El uso de aditivos orgánicos en mezclas de morteros de cal en el área maya, in *La Cal Historia Propiedades Y Usos*, ed. L. B. Pingarrón and I. Villaseñor-Alonso, E-publish, México, 2013, pp. 115–138.
13 K. Zhai, B. Zhang and L. Zhu, A new proposed semi-quantitative method for the organic additives analysis in traditional lime mortar, *J. Cult. Herit.*, 2023, **62**, 284–292.

14 A. G. Ordóñez-Melken, C. B. Rodríguez-Poot, J. A. Gómez-Pinzón and N. M. Navarrete-Canto, *Mortero Arquitectónico a Base de Resina Del Árbol de Chukum*, Ava Cient VII, 2019, pp. 107–114.
15 G. Carnevali Fernández-Concha, J. L. Tapia-Muñoz, R. Duno de Stefano and I. M. Ramírez-Morillo, *Flora ilustrada de la Península de Yucatán: listado florístico*, E-Publish CICY, México, 2010.
16 M. L. Rico-Arce, S. L. Gale and N. Maxted, A taxonomic study of *Albizia* (Leguminosae: Mimosoideae: Ingeae) in México and Central America, *An. Inst. Bot. A. J. Cavanilles*, 2008, **65**(2), 255–305.
17 Y. A. El-Khodary, I. M. Ayoub, S. H. El-Ahmady and N. Ibrahim, Molecular and phytochemical variability among genus *Albizia*: a phylogenetic prospect for future breeding, *Mol. Biol. Rep.*, 2021, **48**, 2619–2628.
18 N. De Belie, J. Lenehan, C. Braam, B. Svennerstedt, M. Richardson and B. Sonck, Durability of building materials and components in the agricultural environment, part III: concrete structures, *J. Agric. Eng. Res.*, 2000, **76**(1), 3–16.
19 S. Hadigheh, R. Gravina and S. T. Smith, Effect of acid attack on FRP-to-concrete bonded interfaces, *Constr. Build. Mater.*, 2017, **152**, 285–303.
20 K. Rashid, M. Ahmad and M. A. Tahir, Influence of organic agents to compressive strength of cement mortar, *Constr. Build. Mater.*, 2018, **175**, 434–438.
21 S. P. Shah, P. Hou and M. S. Konsta-Gdoutos, Nano-modification of cementitious material: toward a stronger and durable concrete, *J. Sustainable Cem.-Based Mater.*, 2016, **5**, 1–22.
22 S. Kawashima, P. Hou, D. J. Corr and S. P. Shah, Modification of cement-based materials with nanoparticles, *Cem. Concr. Compos.*, 2013, **36**, 8–15.
23 M. Oltulu and R. Sahin, Effect of nano-SiO_2, nano-Al_2O_3 and nano-Fe_2O_3 powders on compressive strengths and capillary water absorption of cement mortar containing fly ash: a comparative study, *Energy Build.*, 2013, **58**, 292–301.
24 D. Siang-Ng, S. Chandra-Paul, V. Anggraini, S. Ying-Kong, T. Shams-Qureshi, C. Romero-Rodriguez, Q.-f. Liu and B. Šavija, Influence of SiO_2, TiO_2 and Fe_2O_3 nanoparticles on the properties of fly ash blended cement mortars, *Constr. Build. Mater.*, 2020, **258**, 119627–119638.
25 D. Coffetti, E. Crotti and L. Coppola, Long-term properties of self-cleaning alkali-activated slag-based mortars with titanium dioxide nanoparticles, *Constr. Build. Mater.*, 2023, **392**, 131976–131986.
26 A. Fujishima, X. Zhang and D. A. Tryk, TiO_2 photocatalysis and related surface phenomena, *Surf. Sci. Rep.*, 2008, **63**, 515–582.
27 F. A. Brehm, C. A. Mendes-Moraes, R. C. Espinosa-Modolo, A. C. Faria-Vilela and D. C. Coitinho Dal Molin, Oxide zinc addition in cement paste aiming electric arc furnace dust (EAFD) recycling, *Constr. Build. Mater.*, 2017, **139**, 172–182.
28 F. Ziegler and C. A. Johnson, The solubility of calcium zincate ($CaZn_2(OH)_6 \cdot 2H_2O$), *Cem. Concr. Res.*, 2001, **31**, 1327–1332.
29 NMX-C-530-ONNCCE-2018, Industria de la Construcción – Durabilidad – Norma General de Durabilidad de Estructuras de Concreto Reforzado – Criterios y Especificaciones, Publicada, 2019.
30 NMX-C-077-1997-ONNCCE, Industria de la construcción – Agregados para concreto – Análisis granulométrico, Publicada, 1998.
31 NMX-C-514-ONNCCE-2016, Industria de la construcción – Resistividad eléctrica del concreto hidráulico – Especificaciones y métodos de ensayo, Publicada, 2016.
32 NMX-C-275-ONNCCE-2004, Industria de la construcción – Concreto – Determinación de la velocidad de pulso a través del concreto – Método de ultrasonido. Publicada, 2004.
33 NMX-C-504-ONNCCE-2015, Industria de la construcción – Determinación de la absorción capilar en concreto hidráulico – Método de ensayo, Publicada, 2015.
34 N. Gomez-Ortiz, S. C. De la Rosa-Garcia, W. S. Gonzalez-Gomez, M. Soria-Castro, P. Quintana, G. Oskam and B. O. Ortega-Morales, Antifungal coatings based on $Ca(OH)_2$ mixed with ZnO/TiO_2 nanomaterials for protection of limestone monuments, *ACS Appl. Mater. Interfaces*, 2013, **5**, 1556–1565.
35 Flora digital, *Albizia tomentosa*, **https://www.cicy.mx/sitios/flora%20digital/ficha_virtual.php?especie=1508**, accessed 5 July 2023.
36 S. Brunauer, L. S. Deming, W. E. Deming and E. Teller, On a Theory of the van der Waals Adsorption of Gases, *J. Am. Chem. Soc.*, 1940, **62**, 1723–1732.
37 M. A. Díaz-Díez, V. Gómez-Serrano, C. Fernández-González, E. M. Cuerda-Correa and A. Macías-García, Porous texture of activated carbons prepared by phosphoric acid activation of woods, *Appl. Surf. Sci.*, 2004, **238**, 309–313.
38 E. P. Barret, P. B. Joyner and P. Halenda, The Determination of Pore Volume and Area Distributions in Porous Substances. I. Computations from Nitrogen Isotherms, *J. Am. Chem. Soc.*, 1951, **73**, 373–380.
39 M. Soria-Castro, S. C. De la Rosa-García, P. Quintana, S. Gómez-Cornelio, A. Sierra-Fernández and N. Gómez-Ortíz, Broad spectrum antimicrobial activity of $Ca(Zn(OH)_3)_2 \cdot 2H_2O$ and ZnO nanoparticles synthesized by the sol–gel method, *J Solgel Sci Technol.*, 2019, **89**, 284–294.
40 U. Zagada-Dominguez, S. De la Rosa-García, M. Ruiz-Gómez, R. López-González, M. Soria-Castro, P. Quintana and S. Gómez-Cornelio, Photocatalytic and antifungal activity of $CaZn_2(OH)_6 \cdot 2H_2O$ mixed with $Ca(OH)_2$ for its application in cultural heritage, *J. Photochem. Photobiol., A*, 2020, **392**, 112440–112449.
41 S. Lázaro-Mass, S. C. De la Rosa-García, C. García-Solis, J. Reyes-Trujeque, M. Soria-Castro, P. Quintana and S. Gómez-Cornelio, Controlling growth of phototrophic biofilms on limestone using $CaZn_2(OH)_6 \cdot 2H_2O$ and ZnO Nanoparticles, *J. Chem. Technol. Biotechnol.*, 2022, **97**, 3011–3023.
42 J. Zhang, Z. Kang, Y. Yang, B. Dong and H. Ma, Enhancement of heat-cured cement paste with tannic acid, *Cem. Concr. Compos.*, 2023, **137**, 104931.

43 L. Wang, J. Wang, H. Wang, Y. Fang, W. Shen, P. Chen and Y. Xu, Eco-friendly treatment of recycled concrete fines as supplementary cementitious materials, *Constr. Build. Mater.*, 2022, **322**, 126491.

44 Human Metabolome, Sucrose, **https://hmdb.ca/metabolites/HMDB0000258**, accessed 7 July 2023.

45 M. Natsume, N. Osakabe, M. Oyama, M. Sasaki, S. Baba, Y. Nakamura, T. Osawa and J. Terao, Structures of (−)-Epicatechin Glucuronide Identified from Plasma and Urine after Oral Ingestion of (−)-Epicatechin: Differences between Human and Rat, *Free Radical Biol. Med.*, 2003, **34**, 840–849.

46 H. G. Méndez-Figueroa, M. Soria-Castro, G. I. Hernández-Bolio, L. F. Hernández-Pat, P. Quintana-Owen, R. Galván-Martínez, A. Espinoza-Vázquez and R. Orozco-Cruz, Evaluation of pH-sensitive nanocontainers composed of hierarchical ZnO mesoporous structures loaded with the *Mimosa tenuiflora* extract for applications in a saline solution, *J. Solid State Electrochem.*, 2023, **27**, 3137–3147.

47 L. A. Alonzo-Salomón and L. Espinoza-Graham, Estudio de las propiedades de la roca caliza de Yucatán, *Ingeniería*, 2003, **7**, 27–36.

48 G. Villain, M. Thiery and G. Platre, Measurement methods of carbonation profiles in concrete: thermogravimetry, chemical analysis and gammadensimetry, *Cem. Concr. Res.*, 2007, **37**, 1182–2119.

49 D. Chinh Chu, J. Kleib, M. Amar, M. Benzerzour and N. Abriak, Determination of the degree of hydration of Portland cement using three different approaches: Scanning electron microscopy (SEM-BSE) and Thermogravimetric analysis (TGA), *Case Stud. Constr. Mater.*, 2021, **15**, e00754.

50 G. Aranovich and M. Donohue, Analysis of Adsorption Isotherms: Lattice Theory Predictions, Classification of Isotherms for Gas–Solid Equilibria, and Similarities in Gas and Liquid Adsorption Behavior, *J. Colloid Interface Sci.*, 1998, **200**, 273–290.

51 W. He, Z. Jiao, Y. Wang, J. Xu and Q. Zhao, Research on the mechanical properties and electrical conductivity of cement mortar based on recycled nano-iron boride, *Waste Dispos. Sustain. Energy.*, 2021, **3**, 155–164.

52 T. Dorn, O. Blask and D. Stephan, Acceleration of cement hydration – a review of the working mechanisms, effects on setting time, and compressive strength development of accelerating admixtures, *Constr. Build. Mater.*, 2022, **323**, 126554.

53 H. F. Mahmood, H. Dabbagh and A. A. Mohammed, Comparative study on using chemical and natural admixtures (grape and mulberry extracts) for concrete, *Case Stud. Constr. Mater.*, 2021, **15**, e00699.

54 M. Khazma, N. E. Hajj, A. Goullieux, R. M. Dheilly and M. Queneudec, Influence of sucrose addition on the performance of a lignocellulosic composite with a cementious matrix, *Composites, Part A*, 2008, **39**, 1901–1908.

55 M. Tramontin-Souza, R. Dors-Sakata, L. Onghero, L. Colares-Magalhães, C. E. Maduro de Campos, A. P. Novaes de Oliveira and W. Longuini-Repette, Insights into the "accelerating effect" of sucrose on cement pastes, *J. Build. Eng.*, 2022, **59**, 105053.

56 L. Jiang, W. Ke and Q. Ming-Liang, Experimental determination on the capillary water absorption coefficient of porous building materials: a comparison between the intermittent and continuous absorption tests, *J. Build. Eng.*, 2020, **28**, 10109.

57 P. Castro-Borges and J. M. Mendoza-Rangel, Influence of climate change on concrete durability in Yucatan peninsula, *Corros. Eng., Sci. Technol.*, 2010, **45**, 61–69.

58 H. Umar, D. Kavaz and N. Rizaner, Biosynthesis of zinc oxide nanoparticles using *Albizia lebbeck* stem bark, and evaluation of its antimicrobial, antioxidant, and cytotoxic activities on human breast cancer cell lines, *Int. J. Nanomed.*, 2019, **14**, 87–100.